IEEE Access
Multidisciplinary | Rapid Review | Open Access Journal

Received 15 October 2023, accepted 19 November 2023, date of publication 23 November 2023,
date of current version 29 November 2023.

Digital Object Identifier 10.1109/ACCESS.2023.3336416

RESEARCH ARTICLE

Torque Fault-Tolerant Hierarchical Control of 4WID Electric Vehicles Based on Improved MPC and SMC

XUN HUANG[1], YUNFEI ZHA[1,2], XIAOLONG LV[1], AND XIAOYU QUAN[1]
[1]Fujian Provincial Key Laboratory of Automotive Electronics and Electric Drive, Fujian University of Technology, Fuzhou 350118, China
[2]New Energy Vehicle Motion Control Research Institute, Fujian University of Technology, Fuzhou 350118, China

Corresponding author: Yunfei Zha (fei244@163.com)

This work was supported in part by the Major Science and Technology Program in Fuzhou under Grant 2022-ZD-008, and in part by the Fujian Province Industry Education Cooperation Project under Grant 2023H6019.

ABSTRACT The 4-wheel independent drive (4WID) electric vehicle has better safety and stability. However, the multi-motor drive system would lead to an increased fault probability in the vehicle. In particular, the uncertainty of fault motors and parameter disturbances could lead to uncertainties in control. This study presents a fault-tolerant hierarchical control approach that utilizes an improved Model Predictive Control (MPC) to address the problem. The proposed method employs Sliding Mode Control (SMC) in the upper layer to generate the vehicle's yaw moment, which could inhibit system parameter disturbance and improve the system's robustness. Incorporating the fault matrix induced by motor malfunctions, the state-space equation of the vehicle is modified to establish a vehicle dynamics model under motor faults. In the lower layer, the torque reconstruction allocation strategy is designed to coordinate the four motors under the motor fault condition by the MPC rolling optimization online, which could reduce the impact of the motor fault uncertainty for fault-tolerant control. The multi-constraint conditions of MPC are set up according to the vehicle state parameters. To address the additional yaw moment caused by the MPC torque reconfiguration allocation control strategy, the torque transfer method is used as the input allocation for MPC. Finally, the proposed control strategy is verified by online simulation. The simulation outcomes demonstrate the effectiveness of the proposed hierarchical fault-tolerant control approach in achieving fault-tolerant control of the 4WID electric vehicle, with the improved MPC outperforming the conventional MPC in terms of performance.

INDEX TERMS 4-wheels independent drive electric vehicle, fault-tolerant hierarchical control, failure factor, improved MPC, SMC.

I. INTRODUCTION

Compared to conventional vehicles, the 4-wheel independent drive (4WID) electric vehicle (EV) exhibits superior efficiency and torque control capabilities. Additionally, they possess the ability to collect multi-dimensional vehicle state information, which serves as a foundation for implementing advanced control strategies aimed at achieving complex dynamic control. As a result, 4WID EVs have attracted considerable interest in the realm of vehicle stability control investigation [1], [2], [3], [4], [5].

Due to the large number of motors and poor working environment, the probability of motor faults is relatively high [6]. Significant enhancements have been achieved in the areas of fault tolerance, reliability, and safety of the 4WID EV [7], [8], [9]. In the event of motor failure, it is essential to implement appropriate fault-tolerant control strategies to coordinate torque from healthy motors and prevent vehicle instability, thereby ensuring optimal vehicle dynamic performance [10], [11], [12].

The associate editor coordinating the review of this manuscript and approving it for publication was Xiaosong Hu.

© 2023 The Authors. This work is licensed under a Creative Commons Attribution-NonCommercial-NoDerivatives 4.0 License.
For more information, see https://creativecommons.org/licenses/by-nc-nd/4.0/

The control strategy that enables fault-tolerance in torque can typically be categorized into two types: Passive Fault Tolerant Control (PFTC) and Active Fault Tolerant Control (AFTC) [13], [14]. In PFTC systems, fault diagnosis is not performed online, and instead the fault is either believed to be partially known ahead of time or treated as an extra disturbance. This means that the system does not actively gather and utilize real-time fault diagnosis information. The application of robust control [15] and adaptive control [16] has been employed to ensure handling stability and safety in the event of motor faults in 4-wheel independent drive electric vehicles. There is no need for information on system dynamics parameters and fault detection and identification [17], [18].

The use of Event-Triggered Mechanism (ETM) [19], [20] in AFTC reduces energy usage and system state interaction, but because it may trigger actions within a certain time interval after the event occurs, there is no guarantee of a real-time response when a failure occurs. In contrast, the controller parameters can be reconfigured in this condition with the FD information provided by the AFTC [21], [22], [23]. For example, in [24], Real-time switching control of a multi-control approach can adjust controller parameters to maximize vehicle stability. The reconfigurable controller utilizes insights from motor fault diagnosis to effectively manage the operation of both healthy and faulty motors in a coordinated manner [25], [26], [27], [28]. The reconfigurable control strategy usually coordinates control variables based on the changing system parameters under a motor fault condition. However, the disturbances and system uncertainties can still cause severe impacts on vehicle reconfigurable control. In 4WID EVs, system disturbances and uncertainties can potentially stem from various sources, including but not limited to parameter perturbations and unmodeled dynamics [29], [30]. Therefore, it is necessary to suppress the impact of the disturbances and system uncertainties. In [31], [32], [33], and [34], the application of Sliding Mode Control (SMC) has been utilized to maintain stable vehicle operation in the presence of faults due to its inherent ability to suppress disturbances and its effectiveness in controlling nonlinear systems.

In 4WID EVs, an optimal control allocation approach is needed to distribute torque across the four motors, ensuring coordinated operation of all four motors [35], [36]. The study indicates it could realize the different control objectives with different control allocations. In studies of coordinating the operations of healthy and fault motors, usually direct control allocation [37], pseudoinverse [38], linear programming methods [39],, quadratic programming methods [40] and linear quadratic regulator (LQR) [41] in fault conditions.

To address the system uncertainty caused by motor faults, this study applies Model Predictive Control (MPC) to optimally allocate the motor torque. MPC uses rolling optimization online to inhibit system uncertainty and improve system robustness and stability [42], [43]. Meanwhile, MPC is suitable for the 4WID EV model with parameter time variations due to its multiple inputs, outputs, and constraints. During the operation of the MPC method, the application of motor torque may give rise to an undesired yaw moment. To mitigate this issue, pre-control allocation of the MPC is employed through torque transfer, aimed at preventing the occurrence of additional yaw moments.

In this study, aimed at the fault-tolerant control problem of the 4WID EV drive caused by the uncertainty and degree of motor fault, we propose an FTC algorithm based on improved MPC. Motor faults are treated as disturbances, and fault factors are defined to describe the motor fault state in order to avoid traditional complex fault detection and diagnosis mechanisms [44]. The vehicle control architecture consists of two hierarchical layers. The higher-level layer employs the PID algorithm to achieve speed tracking, while the required yaw moment is obtained through SMC algorithm calculation. In the lower layer, an improved MPC fault-tolerant control strategy is presented. Meanwhile, considering the constraints of control parameters, output parameters, and motor capacity, the control allocation needs to optimally allocate the torques of the healthy motor under the motor fault by rolling optimization. Due to the challenging direct acquisition of the required vehicle state in practical engineering, this study estimates vehicle state using an Unscented Kalman Filter (UKF) observer. Finally, the simulation platform is employed to confirm the effectiveness of the proposed control strategy.

The contributions of this research can be summarized as follows:

1) This study introduces a failure factor to signify the drive motor's failure state. At the same time, a MPC-based torque reconfiguration allocation controller is developed, which transforms the dynamic programming problem into a rolling optimization problem. Through rolling optimization, the deviation of each sampling time is recalculated, allowing us to obtain a locally optimal torque allocation scheme and front wheel angle while considering the constraints imposed by vehicle dynamics.
2) A hybrid strategy that integrates the torque transfer method and the torque allocation method based on objective optimization is deemed more suitable for implementing the fault-tolerant control approach in the presence of complex and variable motor fault conditions. The simulation results demonstrate that, when confronted with motor failure, the proposed improved MPC controller integrated with the torque transfer method exhibits superior performance in terms of vehicle stability control, dynamic behavior, and lateral deviation compared to the single MPC controller.

II. VEHICLE MODEL

A. VEHICLE DYNAMICS MODEL

In order to reduce the complexity of the vehicle model, this research integrates a comprehensive seven-degree-of-freedom vehicle dynamics model, complemented by the inclusion of four-wheel dynamics and a bicycle model. This holistic approach facilitates a more refined depiction and

analysis of the vehicle's motion characteristics, enabling a profound understanding of its intricate dynamics. Only the lateral, longitudinal, and yaw motions, as well as the rotation of the four wheels, are considered in this study. The effects of pitch and roll motions and suspension are neglected. The vehicle dynamic model is shown in Fig. 1.

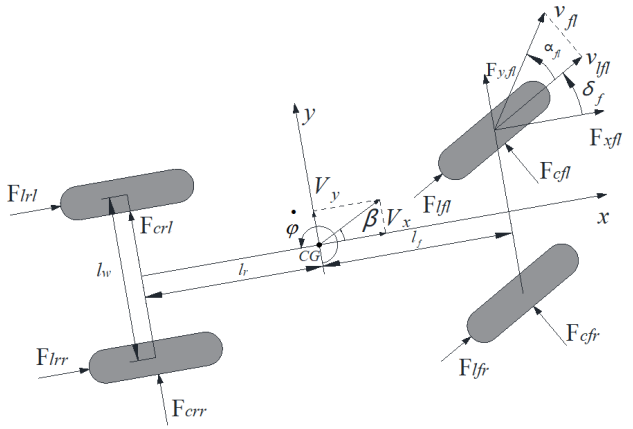

FIGURE 1. Vehicle dynamic model.

According to Figure 1, the dynamic equations governing the lateral and yaw motion of the vehicle can be derived by applying force balance and moment balance as follows:

$$\begin{aligned} m_v\dot{V}_y &= F_{crl} + F_{crr} + (F_{lfl} + F_{lfr})\sin\delta_f \\ &\quad + (F_{cfl} + F_{cfr})\cos\delta_f - m_v\dot{\varphi}V_x \end{aligned} \tag{1}$$

$$\begin{aligned} I_z\ddot{\varphi} &= l_f\left(F_{lfl} + F_{lfr}\right)\sin\delta_f + l_f\left(F_{cfl} + F_{cfr}\right)\cos\delta_f \\ &\quad - l_r\left(F_{crl} + F_{crr}\right) + \frac{l_w}{2}\left(F_{lfr} - F_{lfl}\right)\cos\delta_f \\ &\quad + \frac{l_w}{2}\left(F_{lrr} - F_{lrl}\right) \\ &\quad + \frac{l_w}{2}\left(F_{cfl} - F_{cfr}\right)\sin\delta_f \end{aligned} \tag{2}$$

where m_v is the vehicle mass, δ_f is the front wheels steering angle, I_z refers to the yaw moment of inertia, V_x and V_y is the vehicle's longitudinal and lateral velocities, respectively. F_{lij} and F_{cij} is the wheel's longitudinal and lateral forces, respectively. the subscript i is f and r, representing the front wheel and rear wheel, respectively; the subscript j is l and r, representing the left wheel and right wheel, respectively. l_f is the front wheelbase, l_r is the rear wheelbase, and l_w is the track width. $\dot{\varphi}$ is the yaw rate.

Assuming an accurate description of the vehicle's lateral motion characteristics, the incorporation of elements from the bicycle model is employed within the framework of a simplified model. This approach assumes equal lateral mechanical characteristics for the left and right wheels. The lateral force generated by the wheels can be approximated by the following equations:

$$\begin{cases} F_{cf} = C_f\left(\delta_f - \dfrac{V_y + l_f\cdot\dot{\varphi}}{V_x}\right) \\ F_{cr} = C_r\dfrac{l_r\cdot\dot{\varphi} - V_y}{V_x} \end{cases} \tag{3}$$

where C_f and C_r represent the cornering stiffness of the wheels, respectively.

Taking into account the comprehensive kinematic characteristics and torque distribution of the vehicle's four wheels, the correlation between wheel longitudinal force and torque can be established by employing the tire rotation dynamics model as a basis. The rotational dynamics of the wheels are as follows:

$$J_w\dot{\omega}_{ij} = T_{dij} - T_{bij} - RF_{lij} \tag{4}$$

In this equation, J_w represents the rotational inertia of the wheel. For the sake of simplicity, this paper assumes that the J_w of all four wheels is equal. $\dot{\omega}_{ij}$ is the wheel rotational acceleration of the four wheels, T_{dij} represents the driving torque of the four wheels, R denotes the effective radius of the wheel, while T_{bij} represents the braking torque exerted on each of the four wheels.

By combining Equations (1)-(4), the 7-degree-of-freedom vehicle dynamics model incorporates the tire lateral force representation from the two-wheeled vehicle model and the tire longitudinal force representation from the wheel rotation dynamics. This integration enables the formulation of dynamic equations for the vehicle's lateral and yaw directions, which can be expressed as follows:

$$\dot{V}_y = -\frac{2C_f + 2C_r}{m_vV_x}V_y + \left(\frac{2C_rl_r - 2C_fl_f}{m_vV_x} - V_x\right)\dot{\varphi} + \frac{2C_f\delta_f}{m_v} \tag{5}$$

$$\begin{aligned} \ddot{\varphi} &= \frac{2C_rl_r - 2C_fl_f}{I_zV_x}V_y - \frac{2C_fl_f^2 + 2C_rl_r^2}{I_zV_x}\dot{\varphi} + 2C_fl_f\delta_f \\ &\quad + \frac{l_w}{2RI_z}\left(T_{dfr} - T_{dfl} + T_{drr} - T_{drl}\right) \\ &\quad - \frac{l_w}{2RI_z}\left(T_{bfr} - T_{bfl} + T_{brr} - T_{brl}\right) \\ &\quad - \frac{J_wl_w}{2RI_z}\left(\dot{\omega}_{fr} - \dot{\omega}_{fl} + \dot{\omega}_{rr} - \dot{\omega}_{rl}\right) \end{aligned} \tag{6}$$

B. REFERENCE MODEL

The 2-DOF model is a widely used reference model for vehicle stability analysis that considers the lateral and yaw movements. In this model, the steering angle of the front wheel is considered the input to the system, thereby neglecting the influence of suspension and aerodynamic drag on the vehicle's dynamics. Under steady-state conditions, the mathematical expression of the 2-DOF model is as follows:

$$\dot{\varphi}_{\text{des}} = \frac{V_x}{L + \frac{m_vV_x^2(l_rC_r - l_fC_f)}{2C_fC_rL}}\delta_f \tag{7}$$

where L represents the wheelbase of the vehicle, and $\dot{\varphi}_{des}$ is the desired yaw rate.

The desired yaw rate should adhere to the limitations posed by vehicle speed and ground adhesion conditions, as expressed below:

$$\dot{\varphi}_{\text{max-des}} = \frac{\mu g}{V_x} \tag{8}$$

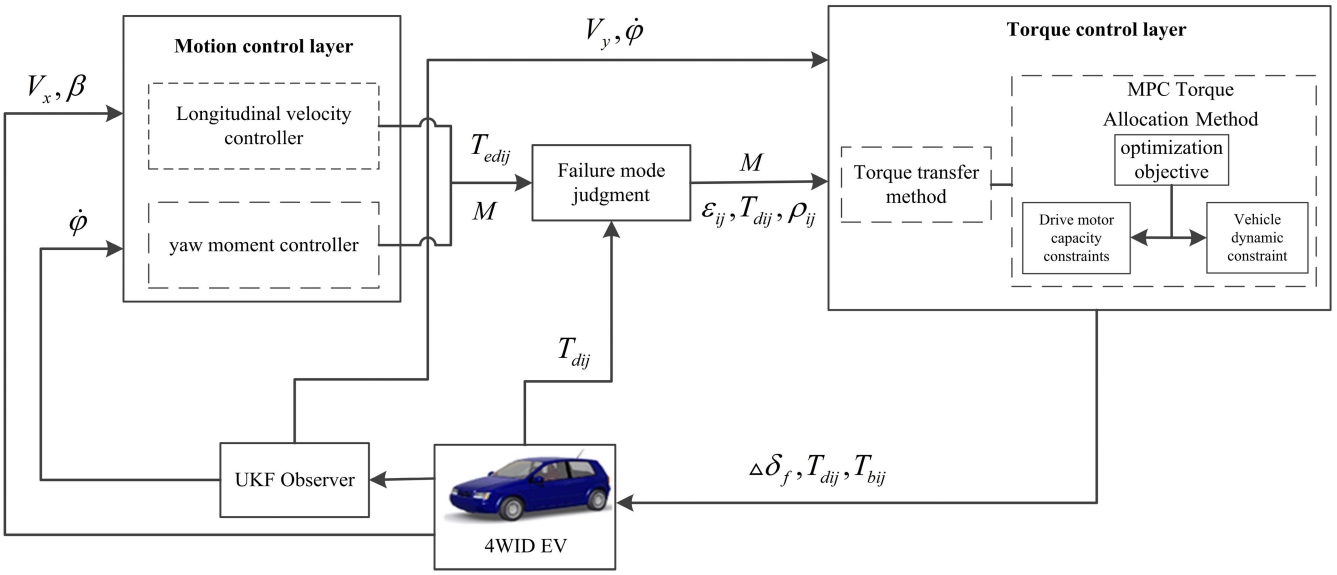

FIGURE 2. Flow chart of drive fault-tolerant control.

where $\dot{\varphi}_{\max -des}$ denotes the upper limit of the yaw rate, whereas μ is the road adhesion coefficient, and g denotes the acceleration due to gravity. For this study, in order to enhance the stability of the vehicle, a reference sideslip angle of zero is established, as a smaller absolute value of the sideslip angle is considered to be more desirable [34]. This assumption is adopted in this study, and determines the upper bound of the desired yaw rate using equation (8).

III. FAULT MODELING OF DRIVE MOTOR

When the motor fails, the motor's power may be completely or partially lost. This requires fault-tolerant controllers to respond quickly to different failures. To make the diagnosis process simpler, more accurately describe the issue, and accelerate the response time, this paper, through the definition of the motor failure and the introduction of the failure factor and braking factor, the motor fault state can be more accurately fed back to the controller so that the controller can redistribute the remaining controllable torque to ensure the vehicle remains in a steady state, i.e., maintaining a constant speed and direction, under various driving conditions.

Equation (9), (10) defines the failure factor ε_{ij} and braking factor ρ_{ij} of the motor:

$$\varepsilon_{ij} = \frac{T_{dij}}{T_{edij}} \tag{9}$$

$$\rho_{ij} = \begin{cases} 1 & \text{When } \varepsilon_{ij} = 0 \\ 0 & \text{When } 0 < \varepsilon_{ij} \leq 1 \end{cases} \tag{10}$$

where T_{edij} and T_{dij} are the desired output torque and the real output torque of the wheel drive motors, respectively. When the failure factor ε_{ij} is 0, the motor of vehicle is completely faulty. In the meantime, ρ_{ij} is 1, which represents the initiation of braking compensation torque to control the stability. When the failure factor $0 < \varepsilon_{ij} < 1$, the motor of vehicle is partially faulty. When the failure factor ε_{ij} is 1, the motor of the vehicle works without a fault. In this condition, ρ_{ij} is 0, and it indicates no braking compensation torque.

Safety becomes paramount in the event of one or more motor failures in 4WID EVs, and compensating for the braking torque should be taken into consideration. Compensation of the braking torque can generate reverse torque to ensure the stable operation of the vehicle, particularly when faults occur in complex road conditions. The driving torque allocation control strategy is used to align the generated yaw moment with the desired yaw moment demand of the upper controller, so that the vehicle has good stability and safety under the premise that it can run stably.

Before the fault of the wheel drive motors, the total driving torque of the four wheels T_e can be equal to the desired driving torque:

$$T_e = T_{dfl} + T_{dfr} + T_{drl} + T_{drr} \tag{11}$$

Insert the failure factor ε_{ij} and braking factor ρ_{ij} into Equation (4), which is rearranged as follows:

$$J_w \dot{\omega}_{ij} = \varepsilon_{ij} T_{dij} - \rho_{ij} T_{bij} - R F_{lij} \tag{12}$$

where, the influences of driving torque, braking torque, failure factor, and braking factor of motors are comprehensively considered. They are used in the state-space model of the driving torque allocation controller below.

Motor faults can be detected through various methods [45]. In this research, the focus is on the FTC of the 4WID EV system. Hence, it assumes that the failure factor εij is already known.

IV. DRIVING TORQUE FAULT-TOLERANT CONTROL STRATEGY

A hierarchical controller is designed to maintain the dynamics and stability of the vehicle when the wheel motor fails.

The control strategy for the vehicle is partitioned into two hierarchical layers, as depicted in Fig. 2. The upper layer is driving torque fault-tolerant controller. The PID algorithm is utilized to design the longitudinal velocity controller, which takes the real and reference values of the longitudinal velocity as inputs and outputs the total driving torque of the hierarchical controller includes the yaw moment and longitudinal velocity controllers. The lower layer is the required by the vehicle. Meanwhile, the SMC method is employed to design the yaw moment controller, which takes the actual and reference values of the yaw rate and center-of-mass sideslip angle as inputs and generates the total desired yaw moment demand of the vehicle. According to the total driving torque output by the upper-layer controller and the torque of the actual four driving motors of the vehicle, the fault is determined through the fault model judgment module, and the failure factor and braking factor are obtained. These factors are output to the lower-level controller together with the vehicle's total desired yaw moment and the torques of the four drive motors. The lower layer of torque fault-tolerant control is designed using a combination of the torque transfer method and the MPC method. Its main function is to reconfigure the desired torque and distribute it to the four-wheel motors. The estimated parameter information of the vehicle is obtained and fed back to the controller by a UKF observer. The optimal control value is obtained through the optimization objective function while incorporating system parameter constraints such as driving torque, front wheel angle, and motor capacity.

A. LONGITUDINAL VELOCITY CONTROLLER

During the operation of a 4WID EV, it is imperative to regulate the vehicle speed to enable prompt response to the driver's intentions. The longitudinal velocity controller computes the overall desired torque by evaluating the disparity between the current velocity of the vehicle and the desired velocity, ensuring that the vehicle has sufficient power. The longitudinal velocity controller is designed to provide feedback of the total torque output to the whole vehicle, realizing closed-loop control of the vehicle velocity.

The longitudinal velocity controller is designed using the PID method, and the model of the longitudinal velocity controller is:

$$T = K_P \cdot \left(V_{t\arg et} - V_x\right) + K_i \cdot \int \left(V_{t\arg et} - V_x\right) dt + K_d \frac{d\left(V_{t\arg et} - V_x\right)}{dt} \tag{13}$$

where T is the desired longitudinal torque, V_{target} is the target longitudinal velocity, K_p, K_i, and K_d are the proportional gain, integral gain, and derivative gain of the PID control algorithm respectively.

The mathematical model of equation (13) can be expressed as:

$$f(\dot{v}) = T$$
$$\dot{e} = V_{t\arg et} - V_x$$

$$T = K_p e + K_i \int e dt + K_d \frac{de}{dt} \tag{14}$$

where $\dot{e}$ is the velocity error.

Define a Lyapunov function:

$$V(e) = \frac{1}{2} e^2 \tag{15}$$

Calculate the time derivative of equation (15):

$$\dot{V}(e) = e\dot{e} = e\left(V_{t\arg et} - V_x\right) \tag{16}$$

According to the Lyapunov stability theorem, if it can be proved that for all e, there is $\dot{V}(e) < 0$, then the system is stable. In this case, the error e will converge to zero.

According to the expression (13) of the output T of the PID controller, $\dot{V}(e)$ can be rewritten as:

$$\begin{aligned}\dot{V}(e) &= e\left(V_{t\arg et} - V_x\right) \\ &= e\left(V_{t\arg et} - K_p e - K_i \int e dt - K_d \frac{de}{dt}\right)\end{aligned} \tag{17}$$

Equation (17) can be simplified as follows:

$$\dot{V}(e) = e\left(V_{t\arg et} - K_p e\right) - K_i e \int e dt - K_d e \frac{de}{dt} \tag{18}$$

By selecting an appropriate gain based on the requirements of $\dot{V}(e) < 0$, it is possible to ensure that expression (18) remains consistently negative, thereby establishing the stability and convergence of the system.

To address the issue of integral saturation, an anti-windup scheme called integral limiting (Anti-Windup) is implemented in the controller. Restricting the output of the integral term within a specific range safeguards the system against instability resulting from the integral term exceeding the adjustable range. The integral term in the PID controller, denoted as $I(t)$, can be susceptible to saturation. To address this, an integral limit value is established to confine the integral term within a predetermined range. Assume that the integral limit is $[-I_{\max}, I_{\max}]$, where $I_{\max}$ is the integral limit.

To solve the calculation of the integral term expressed in I(t), the integral limit method is used:

$$I(t) = I(t-1) + e(t) \cdot dt \tag{19}$$

If the value of I(t) exceeds the defined integral clipping range of $[-I_{\max}, I_{\max}]$, it is constrained to remain within that range:

$$I(t) = \max(\min(I(t), I_{\max}), -I_{\max}) \tag{20}$$

To prevent adverse effects caused by integral saturation and maintain stability and convergence of the tracking error, the value of the integral term I(t) is constrained within the specified range. This constraint ensures that the integral term does not surpass the set limit.

B. YAW MOMENT CONTROLLER

The Sliding Mode Control (SMC) approach exhibits remarkable resistance to nonlinear disturbances, enabling it to achieve superior control performance even in the face of external disturbances and uncertainties. The SMC also responds more quickly to system control inputs when the vehicle malfunctions. The SMC approach adopted in this study leverages the state variable error as the input to synthesize the additional yaw moment, given that the dynamic model is a sophisticated, nonlinear system with high coupling and uncertainty. This strategic approach ensures that the system fulfills the requirements of precise control while maintaining its robustness.

The sliding variable is set as follows:

$$s = (\dot{\varphi} - \dot{\varphi}_{des}) + C(\beta - \beta_{des}) \tag{21}$$

Equation (21) is derived as follows:

$$\dot{s} = \left(\ddot{\varphi} - \ddot{\varphi}_{t\arg et}\right) - C\left(\dot{\beta} - \dot{\beta}_{t\arg et}\right) \tag{22}$$

The expression of the yaw rate in Equation (2) is simplified to:

$$\ddot{\varphi} = \frac{1}{I_z}\begin{bmatrix} l_f\left(F_{cfl} + F_{cfr}\right)\cos\delta_f - l_r\left(F_{crl} + F_{crr}\right) \\ +\left(\cos\delta_f + 1\right)M \end{bmatrix} \tag{23}$$

where, M is the additional yaw-moment.

Equation (22) can be simplified by combining Equation (22) and Equation (23) as follows:

$$\begin{aligned}\dot{s} = &\frac{1}{I_z}\begin{bmatrix} l_f\left(F_{cfl} + F_{cfr}\right)\cos\delta_f - l_r\left(F_{crl} + F_{crr}\right) \\ +\left(\cos\delta_f + 1\right)M \end{bmatrix} \\ &- \ddot{\varphi}_{des} + C\left(\dot{\beta} - \dot{\beta}_{des}\right)\end{aligned} \tag{24}$$

Reducing chattering is an important part of designing an SMC. To enhance the suppression of chatter and convergence speed, a variable exponential reaching law is chosen, represented by the following equation:

$$\dot{s} = -c_1 \cdot \mathrm{sgn}(s) - c_2 \cdot s \tag{25}$$

The Lyapunov function candidate is considered in the SMC. The stability condition of the SMC needs to have a continuous function V:

$$\lim_{|s|\to\infty} V = \infty \tag{26}$$

$$\dot{V} < 0 \, for \; s \neq 0 \tag{27}$$

Let $V = 1/2s^2$, which satisfies Equation (26). The following is the derivative of V with regard to time:

$$\dot{V} = s\dot{s} = -c_1 \cdot s \cdot \mathrm{sgn}(s) - c_2 s^2 \leq 0 \tag{28}$$

Since $\varepsilon \geq 0$, $\dot{V} \leq 0$, which demonstrates the stability of the closed-loop system incorporating the proposed SMC. Based on this, the system's control law may be obtained as follows:

$$\begin{aligned}M = &\frac{I_z}{1 + \cos\delta_f} \\ &\cdot\begin{bmatrix} -\frac{l_f}{I_z}\left(F_{cfl} + F_{cfr}\right)\cos\delta_f + \frac{l_r}{I_z}\left(F_{crl} + F_{crr}\right) \\ -c_1 sgn(s) - c_2 s + \ddot{\varphi}_{t\arg et} - C\left(\dot{\beta} - \dot{\beta}_{t\arg et}\right) \end{bmatrix}\end{aligned} \tag{29}$$

C. DRIVING TORQUE FAULT-TOLERANT CONTROLLER BASED ON IMPROVED MPC

In this study, a fault-tolerant control strategy for driving torque based on improved MPC is proposed. The pre-allocation layer of the driving torque fault-tolerant strategy employs torque transfer, where the output torque of the torque transfer and the desired yaw moment output of the yaw moment controller are used as the MPC controller's inputs. The torque transfer strategy aims to redistribute the torque demand in the case of a failed motor by adding the failed motor's torque demand to the healthy motor on its own side, thereby ensuring the steady state of the vehicle.

The 4WID EV would produce more yaw moment due to the longitudinal force imbalance caused by faults as follows:

$$M_b = \frac{l_w}{2}\left(F_{lfr} + F_{lrr} - F_{lrl} - F_{lfl}\right) \tag{30}$$

where M_b is additional yaw moment to the total longitudinal force.

The torque transfer method is to let M_b be 0, to prevent the additional yaw moment from having an impact on vehicle stability control. Combining Equations (4), (9), (30), the following can be obtained:

$$\varepsilon_{ij}T'_{dfr} + \varepsilon_{ij}T'_{drr} = \varepsilon_{ij}T'_{dfl} + \varepsilon_{ij}T'_{drl} \tag{31}$$

where T'_{dij} is the torque of each motor before the fault.

Based on the feedback from the vehicle motor failure factor and braking factor, the motor fault situation and motor fault location can be determined. The failing driving torque will be superimposed on the same side of the motor without fault. If the total allocated torque surpasses the highest torque produced by a motor, the remaining healthy motors' torque will be reconfigured according to the highest torque produced by the motor, as demonstrated below. T'_{dij} is the torque of each motor without fault, and T_{max} represents the maximum torque produced by a motor.

When the output torque of the same side motor falls below the peak torque, the torque transfer process is shown as the following Equation (32). If the failure factor of the front left wheel is ε_{fl}, then its failure torque would be added to the output torque of the rear left wheel.

$$\begin{cases} T_{dfl} = \varepsilon_{fl}T'_{dfl} \\ T_{dfr} = T'_{dfr} \\ T_{drl} = T'_{drl} + \left(1 - \varepsilon_{fl}\right)T'_{dfl} \\ T_{drr} = T'_{drr} \end{cases} \quad \text{if } T'_{dfr} + T'_{drr} < T_{max} \tag{32}$$

When the output torque of the same side motor exceeds the T_{max}, the torque transfer process is as Equation (33).

$$\begin{cases} T_{dfl} = \varepsilon_{fl}T'_{dfl} \\ T_{dfr} = T'_{dfr} \\ T_{drl} = T_{max} - \varepsilon_{fl}T'_{dfl} \\ T_{drr} = T_{max} - T'_{dfr} \end{cases} \quad \text{if } T'_{dfr} + T'_{drr} > T_{max} \tag{33}$$

where if $\varepsilon_{fl} = 0$, T_{drl} should be the peak torque. Simultaneously, the torque of the right side and left side should be equal based on Equation (31).

Following the failure form analysis in Section III, this paper comprehensively considers the vehicle's driving torque, braking torque, and the influence of fault and braking factors on its yaw stability. By utilizing the torque transfer method to pre-distribute the driving torque, the state space equation required for model predictive control is obtained. On the one hand, the rolling time domain optimization design can ensure the stability of the posture of the 4WID EV. On the other hand, it ensures that the vehicle can meet the dynamic requirements and better ensure the drivers' intentions.

By Combining Equations (1)-(4) and Equations (9), (10), the prediction model can be organized as follows:

$$\dot{V}_y = -\frac{2C_f + 2C_r}{m_v V_x} V_y + \left(\frac{2C_r l_r - 2C_f l_f}{m_v V_x} - V_x\right)\dot{\varphi} + \frac{2C_f \delta_f}{m_v} \tag{34}$$

$$\begin{aligned}\ddot{\varphi} = {} & \frac{2C_r l_r - 2C_f l_f}{I_z V_x} V_y - \frac{2C_f l_f^2 + 2C_r l_r^2}{I_z V_x}\dot{\varphi} + 2C_f l_f \delta_f \\ & + \frac{l_w}{2RI_z}\left(\varepsilon_{fr} T_{dfr} - \varepsilon_{fl} T_{dfl} + \varepsilon_{rr} T_{drr} - \varepsilon_{rl} T_{drl}\right) \\ & - \frac{l_w}{2RI_z}\left(\rho_{fr} T_{bfr} - \rho_{fl} T_{bfl} + \rho_{rr} T_{brr} - \rho_{rl} T_{brl}\right) \\ & - \frac{J_w l_w}{2RI_z}\left(\dot{\omega}_{fr} - \dot{\omega}_{fl} + \dot{\omega}_{rr} - \dot{\omega}_{rl}\right)\end{aligned} \tag{35}$$

The mathematical representation of the system can be expressed as a state-space model:

$$\begin{aligned}\dot{x} &= A_c x + B_{cu} u + B_{cd} d \\ y_c &= C_c x\end{aligned} \tag{36}$$

where the control quantity u of the model is the compensation value of the front wheel angle as well as the driving torque and braking torque, the state x is the lateral velocity and yaw rate, the disturbance d is the four-wheel speed, A_c, B_{cu}, B_{cd}, C_c are coefficient matrices.

$$x = \begin{bmatrix} V_y & \dot{\varphi} \end{bmatrix}^{\mathrm{T}} \tag{37}$$

$$u = \begin{bmatrix} \delta_f & T_{dfr} & T_{dfl} & T_{drr} & T_{drl} & T_{bfr} & T_{bfl} & T_{brr} & T_{drl} \end{bmatrix}^{\mathrm{T}} \tag{38}$$

$$d = \begin{bmatrix} \dot{\omega}_{fr} & \dot{\omega}_{fl} & \dot{\omega}_{rr} & \dot{\omega}_{rl} \end{bmatrix}^{T} \tag{39}$$

Utilizing the current vehicle state feedback, the MPC is implemented to regulate the compensation value of the front wheel angle output as well as the vehicle driving torque, thereby facilitating the closed-loop optimization control of the model. The yaw moment output from the yaw moment controller is the desired value for the lower-layer torque allocation controller. As a result, the predictive model's control output is stated as follows:

$$y_c = \begin{bmatrix} 0 & I_z \end{bmatrix} \begin{bmatrix} V_y \\ \dot{\varphi} \end{bmatrix} \tag{40}$$

The prediction model Equation (36) is expressed as the state-space model, and the coefficient matrix is:

$$A_c = \begin{bmatrix} \frac{2C_f + 2C_r}{m_v V_x} & \frac{2C_r l_r - 2C_f l_f}{m_v V_x} - V_x \\ \frac{2C_r l_r - 2C_f l_f}{I_z V_x} & \frac{2C_f l_f^2 + 2C_r l_r^2}{I_z V_x} \end{bmatrix} \tag{41}$$

$$B_{\mathrm{cu}} = \begin{bmatrix} \frac{2C_f}{m_v} & 0 & 0 & 0 & 0 & 0 & 0 & 0 & 0 \\ 2C_f l_f & e^* & -e^* & e^* & -e^* & -e^* & e^* & -e^* & e^* \end{bmatrix} \tag{42}$$

$$B_{cd} = \begin{bmatrix} 0 & 0 & 0 & 0 \\ -\frac{J_w l_w}{2RI_z} & \frac{J_w l_w}{2RI_z} & -\frac{J_w l_w}{2RI_z} & \frac{J_w l_w}{2RI_z} \end{bmatrix} \tag{43}$$

where $e^* = \frac{l_w}{2RI_z}$.

The discretization of the state-space model allows the coefficient matrix to be changed to:

$$\begin{cases} A = e^{A_c T_S} \\ B_u = \int_0^{T_s} e^{A_c \tau} d\tau \cdot B_{cu} \\ B_d = \int_0^{T_s} e^{A_c \tau} d\tau \cdot B_{cd} \end{cases} \tag{44}$$

where T_s is the sampling time.

Equation (36) represents the transformation of a continuous state-space model into a discrete state-space model, resulting in an incremental model as follows:

$$\begin{aligned}\Delta x(k+1) &= A\Delta x(k) + B_u \Delta u(k) + B_d \Delta d(k); \\ y_c(k) &= C_c \Delta x(k) + y_c(k-1)\end{aligned} \tag{45}$$

At time k, the incremental Equation (46), as shown at the bottom of the next page, of the predictable control state of the prediction model with prediction time domain p as well as the predictable control output Equation (47), as shown at the bottom of the next page, of the prediction model with prediction time domain p are shown at the bottom of this page and at the top of the next page.

The output sequence in the predicted time domain p is specified as:

$$Y_p(k+1|k) = \begin{bmatrix} y_c(k+1|k) \\ y_c(k+2|k) \\ \vdots \\ y_c(k+p|k) \end{bmatrix}_{p\times 1} \tag{48}$$

The input sequence in the control time domain m is defined as:

$$\Delta U(k) = \begin{bmatrix} \Delta u(k) \\ \Delta u(k+1) \\ \vdots \\ \Delta u(k+m-1) \end{bmatrix}_{m\times 1} \tag{49}$$

The failure matrix Q composed of the failure factor and braking factor is set to:

$$Q = \begin{bmatrix} 1 & \varepsilon_{fr} & \varepsilon_{fl} & \varepsilon_{rr} & \varepsilon_{rl} & \rho_{fr} & \rho_{fl} & \rho_{rr} & \rho_{rl} \end{bmatrix} \tag{50}$$

According to Equation (40), the predictive output model is expressed as follows:

$$Y_p(k+1|k) = S_x \Delta x(k) + \mathrm{I} y_c(k) + S_d \Delta d(k) + S_u Q_c \Delta U(k) \tag{51}$$

where coefficient matrix $Q_c = \mathrm{diag}(Q)$. According to the prediction model, the predictive output model Y_p with the prediction time domain p can be calculated by the state increment $\Delta x(k)$, the control quantity $u(k-1|k)$ and the control increment $\Delta U(k)$.

Coefficient matrices S_x, I, S_u, S_d are as (52)–(55), shown at the bottom of the next page.

The reference sequence $R(k+1)$ is the output reference sequence of the upper yaw moment controller at time k, and the reference sequence $R(k+1)$ remains the same in the prediction time domain p. The reference input $R(k+1)$ is defined as:

$$R(k+1) = \left[r(k)\ r(k)\ \cdots\ r(k) \right]^T_{p\times 1} \tag{56}$$

Reducing the four-wheel torque variation rate of a 4WID EV can ensure the torque to change gently. If the deviation of the control reference sequence $R(k+1)$ and the output of the prediction model approaches toward 0, the vehicle's stability can be maintained. Therefore, the optimization function of the optimization objective is set as follows:

$$J = \left\| \Gamma_y \left(Y_p(k+1|k) - R(k+1) \right) \right\|^2 + \left\| \Gamma_u Q_c \Delta U(k) \right\|^2 \tag{57}$$

where Γ_y and Γ_u are the weighted matrices.

At time k, in order to avoid one or more motor faults, the healthy motor output may exceed its saturation limit of higher torque, resulting in deterioration of vehicle performance or loss of vehicle stability. The capacity constraints of the motor and braking should be considered in the constraints. Considering the objective function and constraint conditions, the following optimization needs to be performed:

$$\begin{cases} \min J \\ \triangle U_{\min} \le U(t) \le \triangle U_{\max} \\ U_{\min} \le U(t) + A\triangle U(t) \le U_{\max} \\ y_{\min} \le y \le y_{\max} \\ x_{\min} \le x \le x_{\max} \end{cases} \tag{58}$$

$$\begin{aligned}
\Delta x(k+1|k) &= A\Delta x(k) + B_u \Delta u(k) + B_d \Delta d(k) \\
\Delta x(k+2|k) &= A\Delta x(k+1|k) + B_u \Delta u(k+1) + B_d \Delta d(k+1) = A^2 \Delta x(k) + AB_u \Delta u(k) + AB_d \Delta d(k) + B_u \Delta u(k+1) \\
\Delta x(k+3|k) &= A\Delta x(k+2|k) + B_u \Delta u(k+2) + B_d \Delta d(k+2) = A^3 \Delta x(k) + A^2 B_u \Delta u(k) \\
&\quad + AB_u \Delta u(k+1) + B_u \Delta u(k+2) + A^2 B_d \Delta d(k) \\
&\cdots \\
\Delta x(k+m|k) &= A^{m-1} B_u \Delta u(k) + A^{m-2} B_u \Delta u(k+1) + \cdots + A^{m-1} B_d \Delta d(k) + B_u \Delta u(k+m-1) + A^m \Delta x(k) \\
&\cdots \\
\Delta x(k+p|k) &= A^p \Delta x(k) + A^{p-1} B_u \Delta u(k) + A^{p-2} B_u \Delta u(k+1) + \cdots + A^{p-1} B_d \Delta d(k) + A^{p-m} B_u \Delta u(k+m-1) \\
y_c(k+1|k) &= C_c \Delta x(k+1|k) + y_c(k) = C_c A \Delta x(k) + C_c B_u \Delta u(k) + C_c B_d \Delta d(k) + y_c(k) \\
y_c(k+2|k) &= C_c \Delta x(k+2|k) + y_c(k+1|k) = \left(C_c A^2 + C_c A \right) \Delta x(k) + y_c(k) \\
&\quad + C_c (AB_u + B_u) \Delta u(k) + C_c B_u \Delta u(k+1) + C_c B_d \Delta d(k) \\
&\cdots \\
y_c(k+m|k) &= C_c \Delta x(k+m|k) + y_c(k+m-1|k) = \sum_{i=1}^{m} C_c A^i \Delta x(k) + \sum_{i=1}^{m} C_c A^{i-1} B_u \Delta u(k) \\
&\quad + \sum_{i=1}^{m-1} C_c A^{i-1} B_u \Delta u(k+1) + \cdots + y_c(k) + C_c B_u \Delta u(k+m-1) + \sum_{i=1}^{m-1} C_c A^{i-1} B_d \Delta d(k) \\
&\cdots \\
y_c(k+p|k) &= C_c \Delta x(k+p|k) + y_c(k+p-1|k) = \sum_{i=1}^{p} C_c A^i \Delta x(k) + \sum_{i=1}^{p} C_c A^{i-1} B_u \Delta u(k) \\
&\quad + \sum_{i=1}^{p-1} C_c A^{i-1} B_u \Delta u(k+1) + \cdots + \sum_{i=1}^{p} C_c A^{i-1} B_d \Delta d(k) \\
&\quad + \sum_{i=1}^{p-m+1} C_c A^{i-1} B_u \Delta u(k+m-1) + y_c(k)
\end{aligned} \tag{46, 47}$$

where $\Delta U_{\min}$ and $\Delta U_{\max}$ are the minimum value and maximum value of control increment. y, $y_{\min}$ and $y_{\max}$ are the output of the system and its minimum value and maximum value. x, $x_{\min}$ and $x_{\max}$ are the state of the system and its minimum value and maximum value.

In order to reduce modeling errors, we adopt rolling optimization strategy in the controller design process. In each control cycle, solving the optimization objective function yields the control input sequence, with the sequence's initial piece being applied to the control system. This optimization process is repeated in a rolling manner to form a closed-loop rolling optimization system.

D. UKF OBSERVER

Considering the practical limitations and cost constraints associated with measuring vehicle lateral velocity and yaw rate using complex devices in engineering applications, observers play a crucial role in estimating these parameters. The utilization of a dynamic estimator based on the Unscented Kalman Filter (UKF) allows for real-time estimation of the system under test using readily available sensor information. As a nonlinear filtering algorithm, UKF approximates the probability distribution by calculating a weighted sum of samples, resulting in more accurate estimations. Unlike the Extended Kalman Filter (EKF), UKF circumvents the need to solve the highly nonlinear Jacobian matrix, thereby reducing the complexity and response time of the control model.

In related studies [46], the researchers employed the conventional Kalman filter to achieve an accurate estimation of the sideslip angle. However, UKF demonstrates superior adaptability to system noise and measurement noise, as it can dynamically adjust the covariance matrix to better accommodate real-world noise conditions. This adaptability enables UKF to exhibit better performance in scenarios characterized by noise and uncertainty. Moreover, given the presence of motor failure as a disturbance factor in this study, it is crucial to design a controller that encompasses robustness considerations. UKF, by leveraging unscented transformation, effectively resists interference and minimizes its impact on estimation results. Hence, in this study, UKF was chosen to estimate the lateral vehicle velocity and yaw rate, ensuring accurate and efficient estimation [47]. Combining the vehicle dynamics equation derived above with the UKF algorithm effectively, the state and observation equations of the vehicle system are deduced as:

$$\begin{cases} \dot{\xi}_{UKF}(t) = A_{UKF}\xi_{UKF}(t) + B_{UKF}u_{UKF}(t) \\ z_{UKF}(t) = C_{UKF}\xi_{UKF}(t) + D_{UKF}u_{UKF}(t) \end{cases} \tag{59}$$

where $\xi_{UKF}(t)$ is the state vector of the UKF observer, $\xi_{UKF}(t) = \begin{bmatrix} V_y & \dot{\varphi} \end{bmatrix}^T$, $z_{UKF}(t)$ is the observation vector of the UKF observer, $z_{UKF}(t) = \begin{bmatrix} a_y \end{bmatrix}$, $u_{UKF}(t)$ is the system input, and $u_{UKF}(t) = \begin{bmatrix} \delta_f & F_{lfr} & F_{dfl} & F_{lrr} & F_{lrl} \end{bmatrix}^T$. A_{UKF}, B_{UKF}, C_{UKF}, D_{UKF} are the coefficient matrices of the nonlinear automobile system.

$$A_{UKF} = \begin{bmatrix} -\frac{2C_f+2C_r}{m_v V_x} & \frac{2C_r l_r - 2C_f l_f}{m_v V_x} - V \\ \frac{2C_r l_r - 2C_f l_f}{I_z V_x} & \frac{2C_f l_f^2 + 2C_r l_r^2}{I_z V_x} \end{bmatrix} \tag{60}$$

$$B_{UKF} = \begin{bmatrix} \frac{2C_f}{m_v} & 0 & 0 & 0 & 0 \\ 2C_f l_f & \frac{l_w}{2I_z} & -\frac{l_w}{2I_z} & \frac{l_w}{2I_z} & -\frac{l_w}{2I_z} \end{bmatrix} \tag{61}$$

$$C_{UKF} = \begin{bmatrix} \frac{C_f+C_r}{m_v V_x} & \frac{C_f l_f - C_r l_r}{m_v V_x} \end{bmatrix} \tag{62}$$

$$\mathrm{I} = \begin{bmatrix} \mathrm{I}_{nc\times nc} & \mathrm{I}_{nc\times nc} & \cdots & \mathrm{I}_{nc\times nc} \end{bmatrix}^T_{P\times 1} \tag{52}$$

$$S_x = \begin{bmatrix} C_c A & \sum_{i=1}^{2} C_c A^i & \ldots & \sum_{i=1}^{p} C_c A^i \end{bmatrix}^T_{P\times 1} \tag{53}$$

$$S_d = \begin{bmatrix} C_c B_d & \sum_{i=1}^{2} C_c A^{i-1} B_d & \cdots & \sum_{i=1}^{p} C_c A^{i-1} B_d \end{bmatrix}^T_{p\times 1} \tag{54}$$

$$S_u = \begin{bmatrix} C_c B_u & 0 & 0 & \cdots & 0 \\ \sum_{i=1}^{2} C_c A^{i-1} B_u & C_c B_u & 0 & \cdots & 0 \\ \sum_{i=1}^{3} C_c A^{i-1} B_u & \sum_{i=1}^{2} C_c A^{i-1} B_u & C_c B_u & \cdots & 0 \\ \vdots & \vdots & \vdots & \ddots & \vdots \\ \sum_{i=1}^{m} C_c A^{i-1} B_u & \sum_{i=1}^{m-1} C_c A^{i-1} B_u & \sum_{i=1}^{m-2} C_c A^{i-1} B_u & \cdots & 0 \\ \vdots & \vdots & \vdots & \ddots & \vdots \\ \sum_{i=1}^{p} C_c A^{i-1} B_u & \sum_{i=1}^{p-1} C_c A^{i-1} B_u & \sum_{i=1}^{p-2} C_c A^{i-1} B_u & \cdots & \sum_{i=1}^{p-m+1} C_c A^{i-1} B_u \end{bmatrix}_{p\times m} \tag{55}$$

$$D_{UKF} = \begin{bmatrix} -\frac{C_f}{m_v} & 0 & 0 & 0 & 0 \end{bmatrix} \tag{63}$$

The state space of the vehicle system at time k is:

$$\begin{cases} \xi_{UKF}(k+1) = f(\xi_{UKF}(k)) + w(k) \\ z_{UKF}(k) = h(\xi_{UKF}(k)) + v(k) \end{cases} \tag{64}$$

The vehicle system is represented by a state function $f(\cdot)$ and an observation function $h(\cdot)$, following the equations of the system. $w(k)$ and $v(k)$ are two independent Gaussian white noises. Assuming the estimated state value and variance matrix at the previous time are $\hat{\xi}_{UKF}(k-1)$ and $P_\xi(k-1)$, the UKF filtering system for equation (64) can be implemented using the following specific steps.

1) SETTING THE INITIAL VALUE

$$\begin{cases} \hat{\xi}_{UKF}(0) = E[\xi_{UKF}(0)] \\ P_\xi(0) = E\left\{ \begin{bmatrix} \xi_{UKF}(0) - \hat{\xi}_{UKF}(0) \end{bmatrix} \begin{bmatrix} \xi_{UKF}(0) - \hat{\xi}_{UKF}(0) \end{bmatrix}^T \right\} \end{cases} \tag{65}$$

where $E(\cdot)$ is mathematical expectation.

2) UPDATE TIME

When $k > 1$, construct $2n+1$ sample points:

$$\begin{aligned} \boldsymbol{\chi}(k-1) = \{ & \hat{\xi}_{UKF}(k-1), \hat{\xi}_{UKF}(k-1) \\ & + \left(\sqrt{(n+\lambda)\boldsymbol{P}_\xi(k-1)} \right)_i, \\ & \hat{\xi}_{UKF}(k-1) - \left(\sqrt{(n+\lambda)\boldsymbol{P}_\xi(k-1)} \right)_i \Big\}, i = 1, 2, \cdots, n \end{aligned} \tag{66}$$

where sample point construction methods such as:

$$\boldsymbol{\chi}_i = \begin{cases} \overline{\xi}_{UKF}, & i = 0 \\ \overline{\xi}_{UKF} + \left(\sqrt{(n+l)P_\xi} \right)_i, & i = 1, 2, L, n \\ \overline{\xi}_{UKF} - \left(\sqrt{(n+l)P_\xi} \right)_i, & i = n+1, n+2, L, 2n \end{cases} \tag{67}$$

The weight of each point is shown:

$$w_i^{(a)} = \begin{cases} \dfrac{\lambda}{n+\lambda}, & i = 0 \\ \dfrac{1}{2(n+\lambda)}, & i = 1, 2, \cdots, 2n \end{cases} \tag{68}$$

where λ is a scaling factor employed to mitigate the overall prediction error, and n is the dimensionality of the state vector to be estimated.

The formula for calculating the predicted sample point of the system is:

$$\boldsymbol{\chi}_i^-(k) = f\left(\boldsymbol{\chi}_i(k-1)\right), i = 0, 1, \cdots, 2n \tag{69}$$

The computation of the mean and variance of the predicted sample points can be obtained by utilizing the formulation presented in Equation (70):

$$\begin{cases} \hat{\xi}_{UKF}^-(k) = \sum_{i=0}^{2n} W_i^{(a)} \boldsymbol{\chi}_i^-(k) \\ P_\xi^-(k) = \sum_{i=0}^{2n} W_i^{(a)} \left[\boldsymbol{\chi}_i^-(k) - \hat{\xi}_{UKF}^-(k) \right] \\ \cdot \left[\boldsymbol{\chi}_i^-(k) - \hat{\xi}_{UKF}^-(k) \right]^T + Q_{UKF}(k) \end{cases} \tag{70}$$

where the covariance matrices of the process noise $w(k)$ are set as $Q_{UKF}(k)$.

3) UPDATING MEASUREMENT

If the observed value z(k) is available, the state variables and covariance matrix are updated using equations (71) and (72), respectively:

$$\begin{cases} \hat{\xi}_{UKF}(k) = \hat{\xi}_{UKF}^-(k) + K\left[z(k) - \hat{z}^-(k) \right] \\ P_\xi(k) = P_\xi^-(k) - KP_z(k)K^T \\ K = P_{\xi z}(k) P_z^{-1}(k) \end{cases} \tag{71}$$

$$\begin{cases} \hat{z}^-(k) = \sum_{i=0}^{2n} W_i^{(a)} h\left(\boldsymbol{\chi}_i^-(k)\right) \\ P_z(k) = \sum_{i=0}^{2n} W_i^{(a)} \left[h\left(\boldsymbol{\chi}_i^-(k)\right) - \hat{z}^-(k) \right] \\ \cdot \left[h\left(\boldsymbol{\chi}_i^-(k) - \hat{z}^-(k)\right) \right]^{\mathrm{T}} + R_{UKF}(k) \\ P_{\xi z}(k) = \sum_{i=0}^{2n} W_i^{(a)} \left[\boldsymbol{\chi}_i^-(k) - \hat{\xi}_{UKF}^-(k) \right] \\ \cdot \left[h\left(\boldsymbol{\chi}_i^-(k) - \hat{z}^-(k)\right) \right]^{\mathrm{T}} \end{cases} \tag{72}$$

where the covariance matrices of the observation noise $v(k)$ are set as $R_{UKF}(k)$.

V. SIMULATION ANALYSIS

The suggested fault-tolerant control strategy with improved MPC is compared to the control strategy with MPC to validate the efficacy of the proposed fault-tolerant control strategy with improved MPC. The vehicle dynamic model, torque reconfiguration allocation control, yaw moment control, and motor model are built on the MATLAB/Simulink platform. When combined with the test vehicle, a fault-tolerant control system is jointly established by matching the vehicle parameters with the CarSim model. Choose straight line and double lane settings for the simulation conditions in this investigation. Table 1 displays the simulation of a vehicle's parameters.

A. STRAIGHT LINE SIMULATION

Regarding yaw rate, vehicle speed, and path, the simulation will compare and validate the control effects of these two strategies for vehicle stability, dynamic performance, and tracking ability. Simulation condition 1: Set the vehicle to achieve uniform acceleration in linear motion. The beginning velocity is 60 km/h, while the desired velocity is 80 km/h.

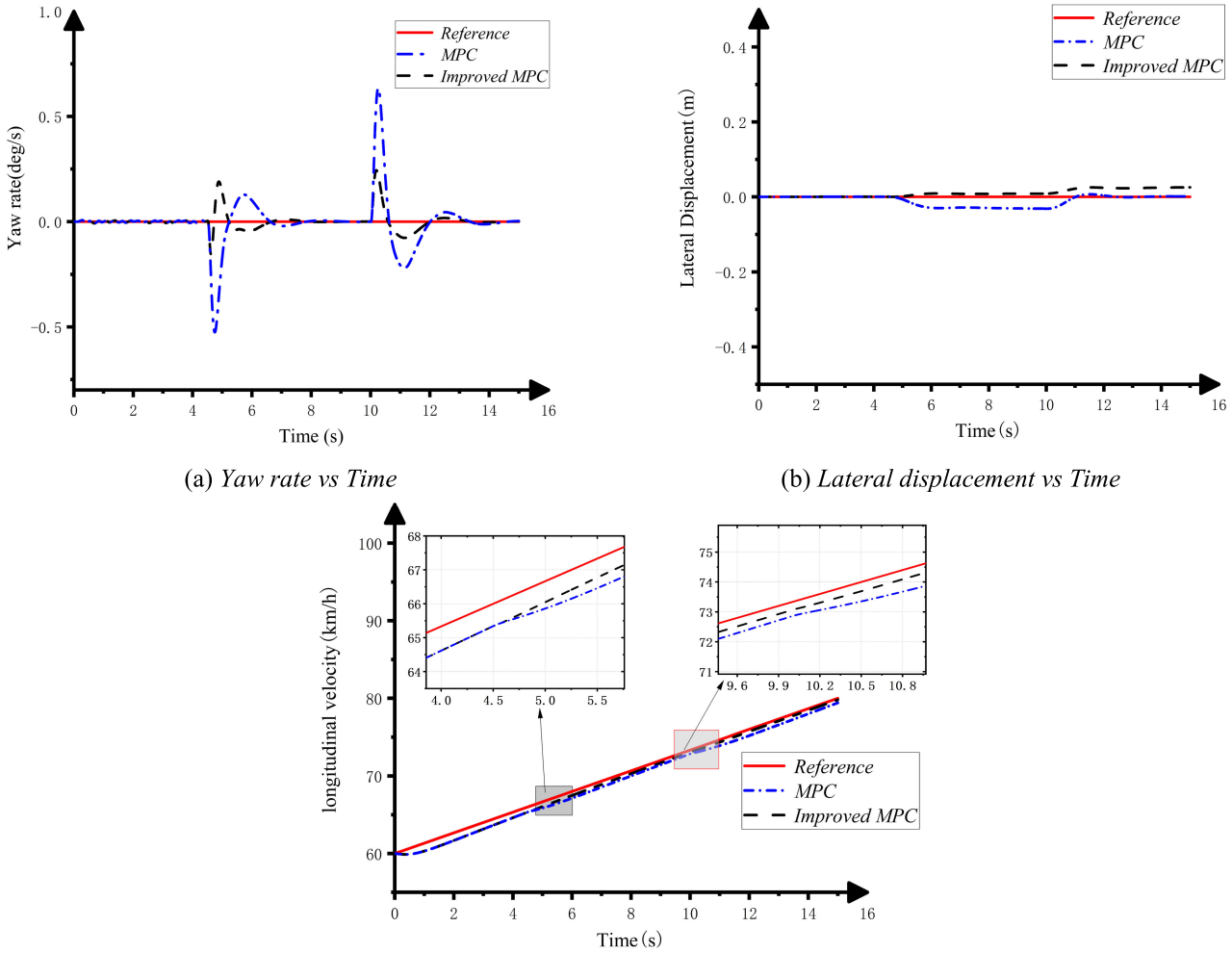

(a) *Yaw rate vs Time*

(b) *Lateral displacement vs Time*

(c) *Longitudinal velocity vs Time*

FIGURE 3. Double fault motor simulation results in straight line.

TABLE 1. 4WID electric vehicle parameters.

Symbol	value	Unit
l_w	1.435	m
m_v	700	kg
l_s	0.43	m
I_z	750	kgm^2
R	0.31	m
l_f	0.945	m
l_r	1.055	m
C_r	62700	N • rad^{-1}
Cf	66900	N • rad^{-1}
T_{max}	120	N·m

The coefficient of road adhesion is 0.85, and the desired yaw rate is 0 (deg/s). After injection at 4.5 s, the right wheel motor completely failed, and then at 10 s, the front left wheel motor partially failed, with a failure factor of 0.5. Figs. 3 and 4 depict the simulation findings. As shown in Fig. 3, when the motors of the rear right wheel and the front left wheel fail, the rest of the motor's torque immediately increases. Then it quickly returns to stability, such that the overall torque remains unchanged to maintain the acceleration characteristics of the vehicle while offsetting the yaw rate bias brought on by the motor defect. It can be seen from Fig. 3 a) that the motor fault has a more obvious influence on vehicle stability under acceleration condition. Under the control of improved MPC, the yaw rate has a fluctuation range of 0.24 deg/s. However, under the control of MPC, the fluctuation range is 0.64 deg/s. It is obvious that the control effect of improved MPC is better under linear acceleration conditions. Under the improved MPC, although the yaw rate fluctuates to a certain extent during the failure of the motor, it quickly returns to stability within 1.5 s. Fig. 3 b) shows the path change curve of the vehicle. There is no severe lateral deviation or instability in the vehicle when the fault occurs. The maximum lateral deviation error of the vehicle under the improved MPC is 0.025 m, whereas the maximum lateral deviation error of the MPC is 0.032 m. Figure 3 c) shows that the improved MPC's speed tracking effect outperforms the fault-tolerant control strategy's sole reliance on the MPC's speed tracking effect for speed tracking, and the dynamic

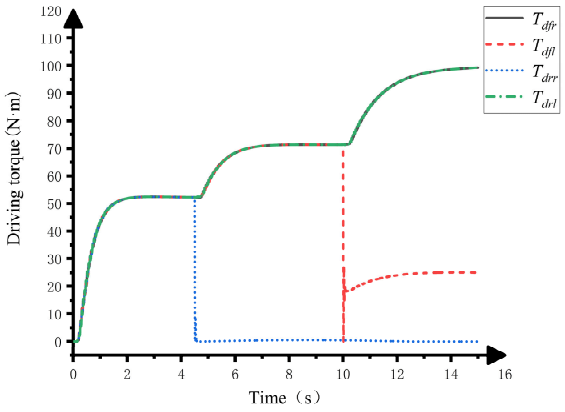

(a) *Four - wheel driving torque curves obtained by MPC*

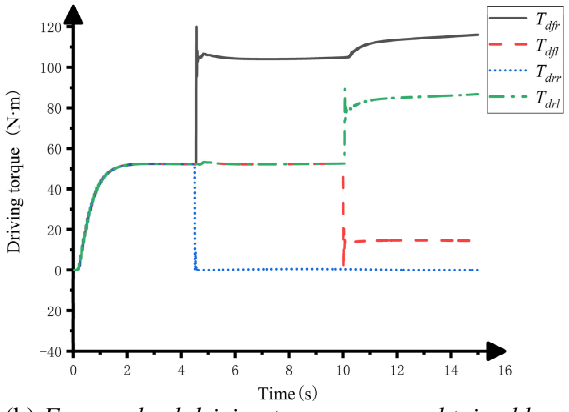

(b) *Four - wheel driving torque curves obtained by improved MPC*

FIGURE 4. Torque variation diagram of double fault motor in straight Line.

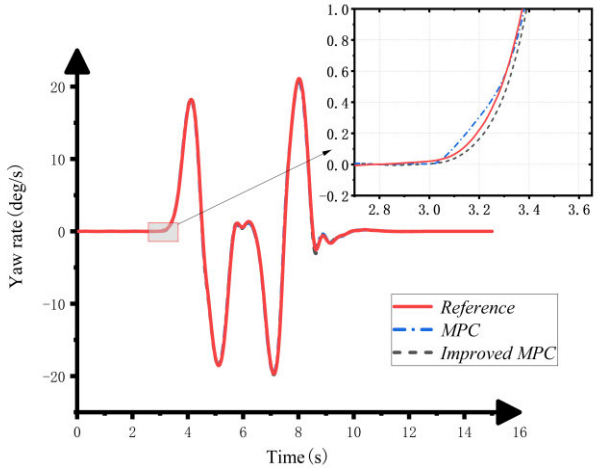

(a) *Yaw rate vs Time*

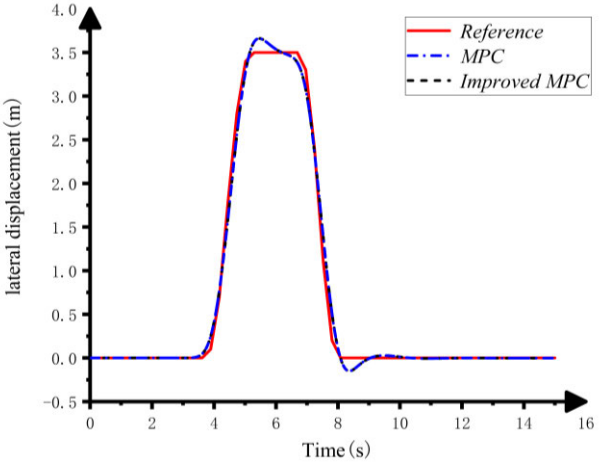

(b) *Lateral displacement vs Time*

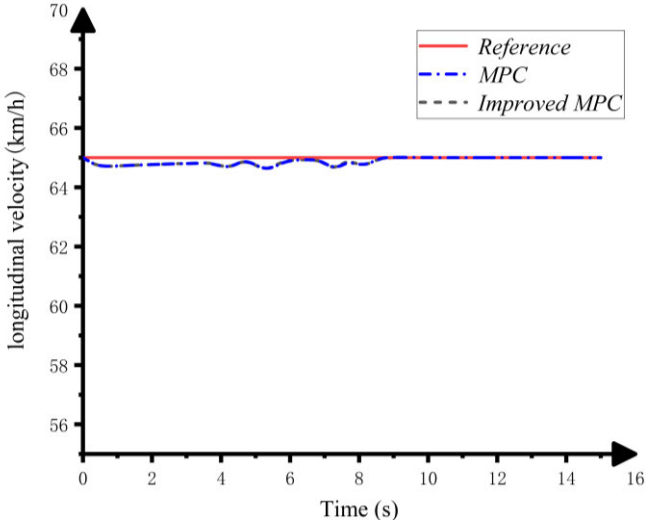

(c) *Longitudinal velocity vs Time*

FIGURE 5. Single fault motor simulation results in double lane change.

performance is better maintained. The speed changes gently and not sharply, and the speed under control basically does not deviate from the ideal speed. During this process, the longitudinal velocity tracking controller operates steadily. The power loss of the MPC fault-tolerant control strategy is relatively larger. It demonstrates that the vehicle can continue

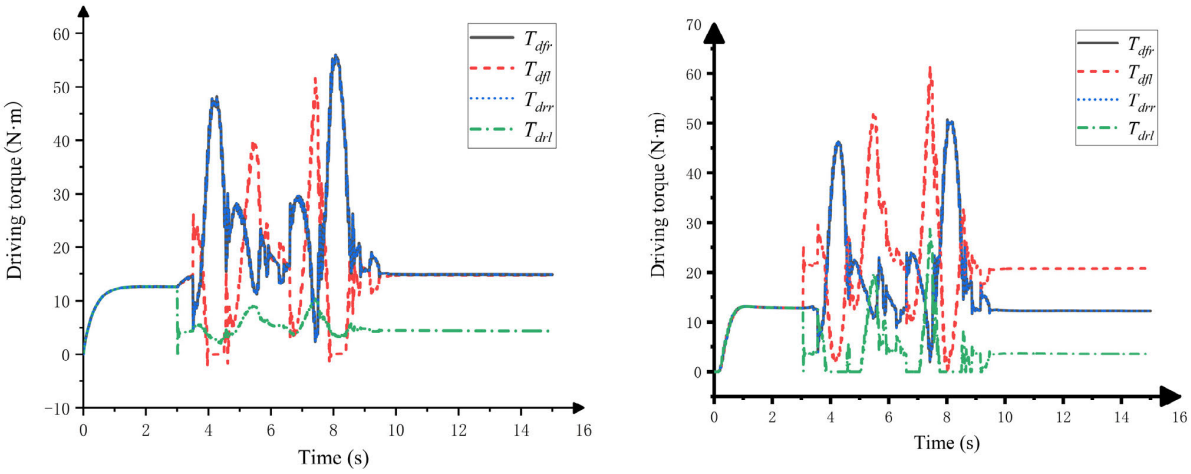

(a) *Four - wheel driving torque curves obtained by MPC*

(b) *Four - wheel driving torque curves obtained by improved MPC*

FIGURE 6. **Torque variation diagram of single fault motor in double lane change.**

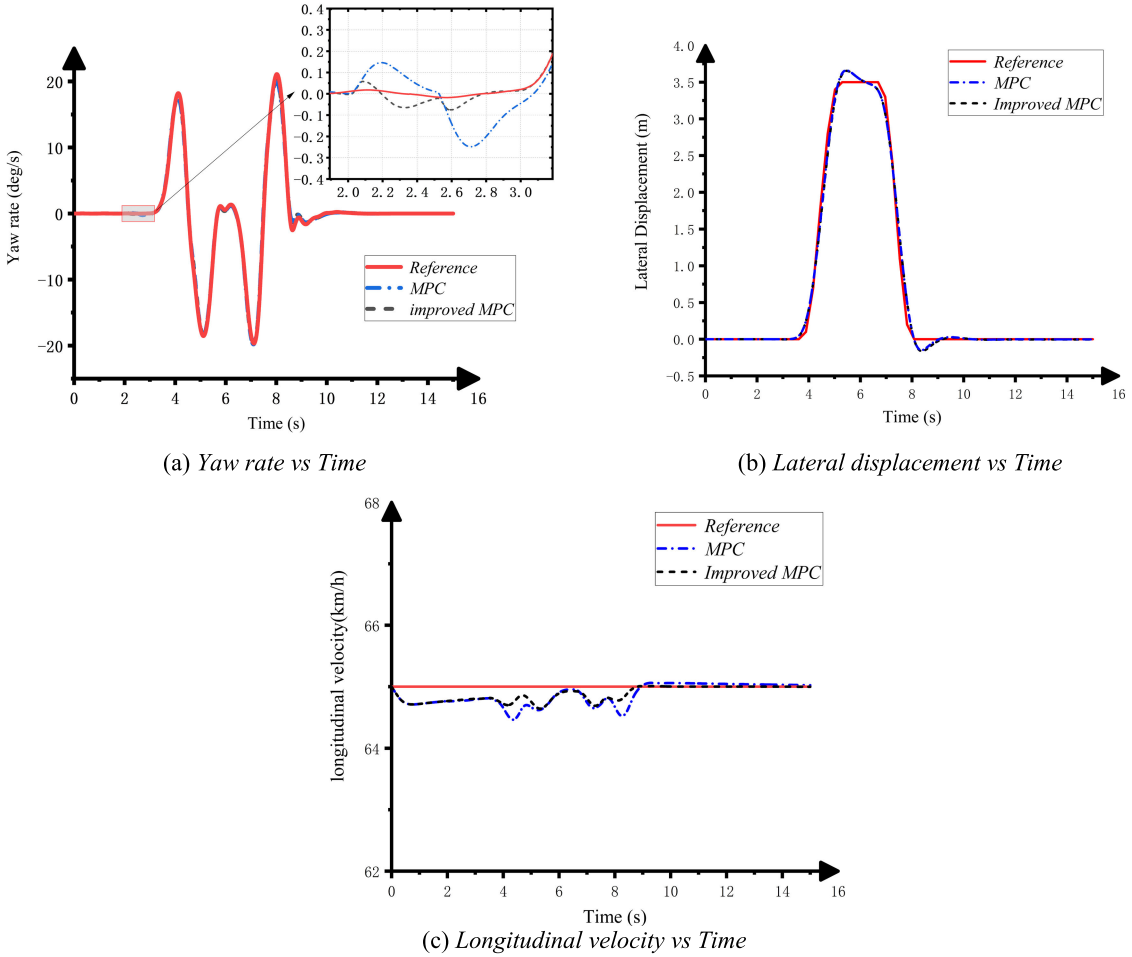

(a) *Yaw rate vs Time*

(b) *Lateral displacement vs Time*

(c) *Longitudinal velocity vs Time*

FIGURE 7. **Double fault motors simulation results in double lane change.**

to go along the desired route even after the motor has failed, while still maintaining good dynamics and handling stability.

Figs. 4 a) and b) show the torque change curves of the four drive motors after two fault-tolerant controls, respectively. When the motor located at the right rear wheel fails, the generated output torque of the motor diminishes to zero. In accordance with Fig. 4 a), under MPC fault-tolerant control, the missing torque is evenly distributed to the remaining

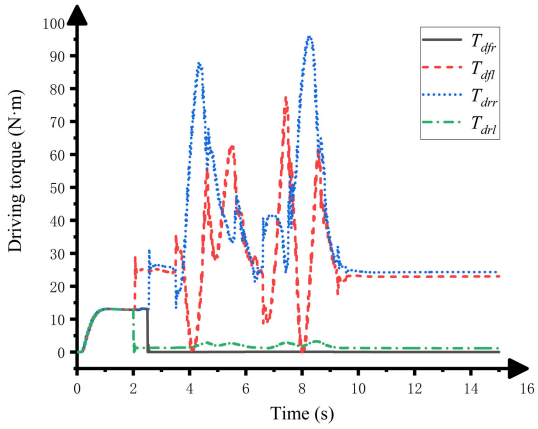

(a) *Four - wheel driving torque curves obtained by improved MPC*

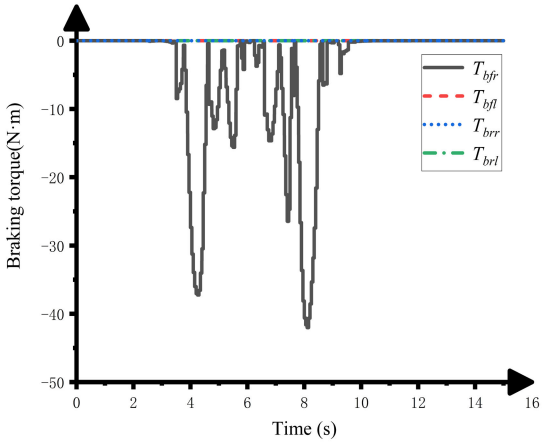

(b) *Four - wheel braking torque curves obtained by improved MPC*

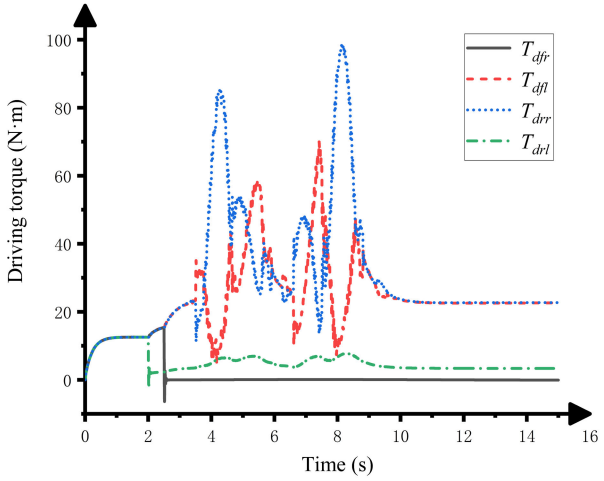

(c) *Four - wheel driving torque curves obtained by MPC*

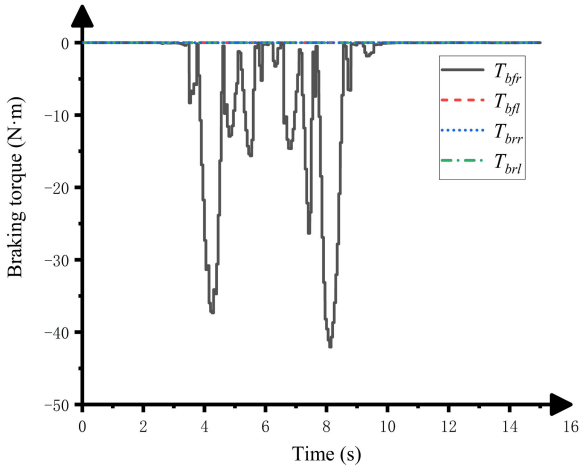

(d) *Four - wheel braking torques curves obtained by MPC*

FIGURE 8. **Torque variation diagram of double fault motors in double lane change.**

three intact motors to maintain the target speed. This control method generates additional yaw moment, which has an impact on the car's stability. Fig. 4 b) shows that under the improved MPC fault-tolerant control, the torque of the same-side off-axis motor is increased to compensate for the power loss. This control scheme makes the driving torque well balanced.

B. DOUBLE LANE SIMULATION

Simulation condition 2: Setting the double line change simulation condition, the coefficient of road adhesion is 0.85, and the beginning velocity is 65 km/h for constant speed. The rear left wheel's failure factor is set at 0.3 at 3 s. Figs. 6 and 7 depict the simulation findings.

As shown in Fig. 5, the yaw rate also fluctuates slightly when the driving torque of the rear left motor suddenly drops to 0.3 times the desired driving torque at 3 s. The yaw rate fluctuation range with MPC is 0.09 deg/s, and 0.1 deg/s with improved MPC. The maximum yaw rate is 20.71 deg/s after a fault occurs and the MPC torque allocation controller reconfigures the driving torque. The fluctuation error of the yaw rate caused by the fault is less than 0.42 %. After the fault-tolerant reconfiguration allocation of the improved MPC, the maximum is 21.10 deg/s and the fluctuation error is lower than 0.43 %. The control effect compared with the two methods for the single motor fault part is similar, which can prove fault-tolerant control method can maintain the vehicle's stability faster under the fault condition. Meanwhile, the vehicle can effectively ensure the safety of the driver. Fig. 5 b) shows lateral displacement curves. When the fault occurs, there is no serious lateral deviation or instability. With the fault-tolerant control strategy of the improved MPC, the maximum error of the lateral deviation is 0.27 m, while that of the MPC is 0.31 m, indicating that the improved MPC's fault-tolerant control strategy performs more dynamically and tracks more accurately. Fig. 5 c) shows the speed variation curves. It is evident that the speed variation with the two fault-tolerant strategies is gentle and not severe. During this

TABLE 2. Simulation results maximum absolute error statistics.

	Simulation condition	*improved MPC*	*MPC*	*Improving degree* (%)
Yaw rate(deg/s)	1	0.24	0.64	62.5
	2	0.77	1.01	23.8
	3	0.07	0.24	70.8
Lateral displacement(m)	1	0.025	0.032	21.9
	2	0.25	0.31	19.4
	3	0.31	0.32	3.1
Longitudinal velocity(km/h)	1	0.42	0.71	40.8
	2	0.30	0.36	16.7
	3	0.35	0.54	35.2

process, the longitudinal velocity tracking controller operates steadily. The maximum fluctuation error of the speed of the control strategy with improved MPC is 0.30 km/h, and that with MPC is 0.36 km/h. Fig. 6 shows that the performance of fault-tolerant control is similar when the two fault-tolerant control strategies are compared because of the partial fault of a single motor, although the difference between the two fault-tolerant control strategies in torque allocation control is due to motor faults.

To test the fault-tolerant controller's effectiveness under various fault conditions, the simulation condition 3 is set as follows: the failure factor of the rear left motor is set as 0.1 at 2 s, and that of the front right motor is set as 0 at 2.5 s. The simulation results are illustrated in Figs. 7 and 8.

As shown in Fig. 7, the fault-tolerant control process can successfully deal with the different fault conditions of the motor. The controller adopts braking compensation torque to keep the vehicle stable at 2.5 s, when the front right motor fails. After the vehicle fails at 2.5 s, the yaw rate fluctuates, which is controlled by the MPC fault-tolerant controller and has a fluctuation range of 0.24 deg/s. With the fault-tolerant control, the maximum yaw rate is 20.00 deg/s, and the fluctuation error of the yaw rate caused by the fault is less than 1.21 %. The yaw rate's range of fluctuation for drive fault-tolerant control using improved MPC is 0.07 deg/s, the maximum is 20.12 deg/s, and the fluctuation error is smaller than 0.35 %. During this process, the longitudinal velocity tracking controller operates steadily. The data comparison in the diagram demonstrates that the improved MPC fault-tolerant method has a better control effect for more complex fault conditions. Fig. 7 b) depicts the vehicle path variation curve. The maximum lateral error of the path using the improved MPC is 0.31 m, and the MPC fault-tolerant control strategy is 0.32 m. The fault-tolerant control strategy using improved MPC has been shown to be superior to the fault-tolerant control strategy using MPC only in the case of double motor failure in terms of meeting dynamic demand under motor faults and maintaining the vehicle's stability. Fig. 8 c) depicts the vehicle longitudinal speed curves. The maximum speed fluctuation error of the fault-tolerant control strategy using improved MPC is 0.35 km/h, and that using MPC is 0.54 km/h. Figs. 8 a) and 8 b) are the four-wheel driving torque curves and the four-wheel braking compensation torque curves with improved MPC, respectively. Figs. 8 c) and 8 d) are the four-wheel driving torque curves and the four-wheel braking compensation torque curves with MPC, respectively. Figs. 8 b) and 8 d) are the braking compensation torque curves with two fault-tolerant strategies that are set as the control output in the torque allocation layer. To guarantee the vehicle's stability under complex fault conditions, it can be possible to dynamically control the braking compensation torque by observing the vehicle's driving state.

Under the three simulation conditions, Table 2 shows the maximum absolute error between the results obtained by the two controllers and the reference value and the degree of improvement compared with the two controllers. Compared with MPC, the improved MPC fault-tolerant control method reduces the yaw rate deviation by 70.8 % at most and 23.8 % at least. The path deviation is reduced by 21.9 % at most and 3.1 % at least. The longitudinal velocity deviation is reduced by 40.8 % at most and 16.7 % at least. It is clear that the improved MPC fault-tolerant control method enhanced stability and the fault-tolerant control effect. At the same time, it can be seen from the above three sets of experiments that the improved MPC fault-tolerant control method has strong robustness and real-time response characteristics.

VI. CONCLUSION

This paper primarily focuses on addressing the issue of faulty drive motors in distributed electric vehicles and investigates control strategies for the motion control layer and fault-tolerant control layer. To ensure driver safety in the event of drive motor failure while maintaining the stability of distributed electric vehicle operation. The main conclusions obtained are as follows:

1) A layered control strategy is designed to address the issue of fault-tolerant control in 4WID electric vehicles, with a focus on torque transmission and rolling optimization. Utilizing the sliding mode variable structure control theory, the control system tracks the desired yaw rate and side slip angle and outputs the desired yaw moment to ensure vehicle stability and safety. Additionally, to prevent the vehicle from losing power, a PID controller is established to output the expected driving torque, and the longitudinal speed tracking of the vehicle under the condition of motor failure is realized.

2) Acknowledging the limitations of the conventional four-wheel torque distribution control method in handling failure modes, this study introduces a failure factor to signify the drive motor's failure state and proposes an improved MPC controller. Based on the motor capacity and vehicle dynamics specifications, a constraint matrix is constructed to attain the desired yaw moment and ensure smooth control variable transitions. In the event of drive motor failure, the optimal solution for coupling control of torque reconstruction and front wheel rotation is achieved.
3) Simulations are performed to assess the efficacy of the improved model predictive control (MPC) fault-tolerant control technique in both straight-lane and double-lane change scenarios. The simulation results demonstrate that the improved MPC fault-tolerant control strategy exhibits superior adaptability and stability in mitigating various motor faults. In comparison to the traditional MPC fault-tolerant control strategy, the proposed approach can better ensure dynamic performance and vehicle stability.

In conclusion, this paper presents a hybrid strategy that integrates the torque transfer method and the target optimization-based torque distribution method. This hybrid strategy is devised to effectively handle diverse and dynamic motor fault conditions. Future research endeavors could enhance this strategy by integrating aspects like vehicle economy and braking energy recovery systems.

REFERENCES

[1] P. Hang, X. Xia, and X. Chen, "Handling stability advancement with 4WS and DYC coordinated control: A gain-scheduled robust control approach," *IEEE Trans. Veh. Technol.*, vol. 70, no. 4, pp. 3164–3174, Apr. 2021, doi: 10.1109/TVT.2021.3065106.

[2] Y. Zha, X. Quan, F. Ma, G. Liu, X. Zheng, and M. Yu, "Stability control for a four-wheel-independent-drive electric vehicle based on model predictive control," *SAE Int. J. Vehicle Dyn., Stability, NVH*, vol. 5, no. 2, pp. 191–204, Mar. 2021, doi: 10.4271/10-05-02-0013.

[3] R. Eto, K. Sakata, and J. Yamakawa, "Driving force distribution based on tyre energy for independent wheel-drive vehicle on rough ground," *J. Terramechanics*, vol. 76, pp. 29–38, Apr. 2018, doi: 10.1016/j.jterra.2017.10.007.

[4] W. Liu, X. Xia, L. Xiong, Y. Lu, L. Gao, and Z. Yu, "Automated vehicle sideslip angle estimation considering signal measurement characteristic," *IEEE Sensors J.*, vol. 21, no. 19, pp. 21675–21687, Oct. 2021, doi: 10.1109/JSEN.2021.3059050.

[5] X. Xia, P. Hang, N. Xu, Y. Huang, L. Xiong, and Z. Yu, "Advancing estimation accuracy of sideslip angle by fusing vehicle kinematics and dynamics information with fuzzy logic," *IEEE Trans. Veh. Technol.*, vol. 70, no. 7, pp. 6577–6590, Jul. 2021, doi: 10.1109/TVT.2021.3086095.

[6] X. Hu, K. Zhang, K. Liu, X. Lin, S. Dey, and S. Onori, "Advanced fault diagnosis for lithium-ion battery systems: A review of fault mechanisms, fault features, and diagnosis procedures," *IEEE Ind. Electron. Mag.*, vol. 14, no. 3, pp. 65–91, Sep. 2020.

[7] D. Zhang, G. Liu, H. Zhou, and W. Zhao, "Adaptive sliding mode fault-tolerant coordination control for four-wheel independently driven electric vehicles," *IEEE Trans. Ind. Electron.*, vol. 65, no. 11, pp. 9090–9100, Nov. 2018, doi: 10.1109/TIE.2018.2798571.

[8] G. Tian, G. Yuan, A. Aleksandrov, T. Zhang, Z. Li, A. M. Fathollahi-Fard, and M. Ivanov, "Recycling of spent lithium-ion batteries: A comprehensive review for identification of main challenges and future research trends," *Sustain. Energy Technol. Assessments*, vol. 53, Oct. 2022, Art. no. 102447, doi: 10.1016/j.seta.2022.102447.

[9] H. Peng, W. Wang, C. Xiang, L. Li, and X. Wang, "Torque coordinated control of four in-wheel motor independent-drive vehicles with consideration of the safety and economy," *IEEE Trans. Veh. Technol.*, vol. 68, no. 10, pp. 9604–9618, Oct. 2019, doi: 10.1109/TVT.2019.2935617.

[10] L. Zhang, H. Ding, Y. Huang, H. Chen, K. Guo, and Q. Li, "An analytical approach to improve vehicle maneuverability via torque vectoring control: Theoretical study and experimental validation," *IEEE Trans. Veh. Technol.*, vol. 68, no. 5, pp. 4514–4526, May 2019, doi: 10.1109/TVT.2019.2903872.

[11] K. Witkowski, G. Kudra, S. Skurativskyi, G. Wasilewski, and J. Awrejcewicz, "Modeling and dynamics analysis of a forced two-degree-of-freedom mechanical oscillator with magnetic springs," *Mech. Syst. Signal Proc.*, vol. 148, Feb. 2021, Art. no. 107138, doi: 10.1016/j.ymssp.2020.107138.

[12] J. Wang, Z. Luo, Y. Wang, B. Yang, and F. Assadian, "Coordination control of differential drive assist steering and vehicle stability control for four-wheel-independent-drive EV," *IEEE Trans. Veh. Technol.*, vol. 67, no. 12, pp. 11453–11467, Dec. 2018.

[13] H. Zhou, F. Jia, Z. Liu, and H. Liu, "Fault diagnosis and fault tolerant control method for in-wheel motor electric vehicles," *J. Mech. Eng.*, vol. 55, no. 22, pp. 174–182, Apr. 2019, doi: 10.3901/JME.2019.22.174.

[14] Y. Wu, G. Zhang, and L.-B. Wu, "Event-triggered adaptive fault-tolerant control for nonaffine uncertain systems with output tracking errors constraints," *IEEE Trans. Fuzzy Syst.*, vol. 30, no. 6, pp. 1750–1761, Jun. 2022, doi: 10.1109/TFUZZ.2021.3065538.

[15] J.-S. Hu, Y. Wang, H. Fujimoto, and Y. Hori, "Robust yaw stability control for in-wheel motor electric vehicles," *IEEE/ASME Trans. Mechatronics*, vol. 22, no. 3, pp. 1360–1370, Jun. 2017, doi: 10.1109/TMECH.2017.2677998.

[16] T. Chen, L. Chen, X. Xu, Y. Cai, H. Jiang, and X. Sun, "Passive fault-tolerant path following control of autonomous distributed drive electric vehicle considering steering system fault," *Mech. Syst. Signal Process.*, vol. 123, pp. 298–315, May 2019, doi: 10.1016/j.ymssp.2019.01.019.

[17] T. Han, Q. Hu, H.-S. Shin, A. Tsourdos, and M. Xin, "Incremental twisting fault tolerant control for hypersonic vehicles with partial model knowledge," *IEEE Trans. Ind. Informat.*, vol. 18, no. 2, pp. 1050–1060, Feb. 2022, doi: 10.1109/TII.2021.3080303.

[18] C. Huang, C. Lv, P. Hang, and Y. Xing, "Toward safe and personalized autonomous driving: Decision-making and motion control with DPF and CDT techniques," *IEEE/ASME Trans. Mechatronics*, vol. 26, no. 2, pp. 611–620, Apr. 2021, doi: 10.1109/TMECH.2021.3053248.

[19] Q. Hou and J. Dong, "Cooperative fault-tolerant output regulation of linear heterogeneous multiagent systems via an adaptive dynamic event-triggered mechanism," *IEEE Trans. Cybern.*, vol. 53, no. 8, pp. 5299–5310, Sep. 2022.

[20] Q. Hou and J. Dong, "Robust adaptive event-triggered fault-tolerant consensus control of multiagent systems with a positive minimum interevent time," *IEEE Trans. Syst., Man, Cybern., Syst.*, vol. 53, no. 7, pp. 4003–4014, Oct. 2023.

[21] B. Guo and Y. Chen, "Robust adaptive fault-tolerant control of four-wheel independently actuated electric vehicles," *IEEE Trans. Ind. Informat.*, vol. 16, no. 5, pp. 2882–2894, May 2020, doi: 10.1109/TII.2018.2889292.

[22] F. Boem, A. J. Gallo, D. M. Raimondo, and T. Parisini, "Distributed fault-tolerant control of large-scale systems: An active fault diagnosis approach," *IEEE Trans. Control Netw. Syst.*, vol. 7, no. 1, pp. 288–301, Mar. 2020, doi: 10.1109/TCNS.2019.2913557.

[23] H. Tang, Y. Chen, and A. Zhou, "Actuator fault-tolerant control for four-wheel-drive-by-wire electric vehicle," *IEEE Trans. Transport. Electrific.*, vol. 8, no. 2, pp. 2361–2373, Jun. 2022, doi: 10.1109/TTE.2021.3136893.

[24] Z. Lei, Y. Wen, W. Zhenpo, and D. Xiaolin, "Fault tolerant control based on multi-methods switching for four-wheel-independently-actuated electric vehicles," *J. Mech. Eng.*, vol. 56, no. 16, p. 227, Apr. 2020, doi: 10.3901/jme.2020.16.227.

[25] H. Dai, P. Chen, and H. Yang, "Metalearning-based fault-tolerant control for skid steering vehicles under actuator fault conditions," *Sensors*, vol. 22, no. 3, p. 845, Jan. 2022, doi: 10.3390/s22030845.

[26] M. Ma, R. Wang, F. Li, J. Wang, and S. Yang, "A fault-tolerant control strategy for switched reluctance motor drive for electric vehicles under short-fault condition," *Microelectron. Rel.*, vol. 88, pp. 1221–1225, Jul. 2018, doi: 10.1016/j.microrel.2018.07.033.

[27] B. Zhao, N. Xu, H. Chen, K. Guo, and Y. Huang, "Stability control of electric vehicles with in-wheel motors by considering tire slip energy," *Mech. Syst. Signal Process.*, vol. 118, pp. 340–359, Mar. 2019, doi: 10.1016/j.ymssp.2018.08.037.

[28] H. Liu, S. Yan, Y. Shen, C. Li, Y. Zhang, and F. Hussain, "Model predictive control system based on direct yaw moment control for 4WID self-steering agriculture vehicle," *Int. J. Agricult. Biol. Eng.*, vol. 14, no. 2, pp. 175–181, Jul. 2021, doi: 10.25165/j.ijabe.20211402.5283.

[29] L. Sun, "Adaptive fault-tolerant constrained control of cooperative spacecraft rendezvous and docking," *IEEE Trans. Ind. Electron.*, vol. 67, no. 4, pp. 3107–3115, Apr. 2020, doi: 10.1109/TIE.2019.2913826.

[30] L. S. Liu, J.-F. Lin, J.-X. Yao, D.-W. He, J.-S. Zheng, J. Huang, and P. Shi, "Path planning for smart car based on Dijkstra algorithm and dynamic window approach," *Wireless Commun. Mobile Comput.*, vol. 4, pp. 1–12, Feb. 2021, doi: 10.1155/2021/8881684.

[31] D. Yin, N. Sun, and J.-S. Hu, "A wheel slip control approach integrated with electronic stability control for decentralized drive electric vehicles," *IEEE Trans. Ind. Informat.*, vol. 15, no. 4, pp. 2244–2252, Apr. 2019, doi: 10.1109/TII.2019.2895371.

[32] Y. Jiang, H. Meng, G. Chen, C. Yang, X. Xu, L. Zhang, and H. Xu, "Differential-steering based path tracking control and energy-saving torque distribution strategy of 6WID unmanned ground vehicle," *Energy*, vol. 254, Sep. 2022, Art. no. 124209, doi: 10.1016/j.energy.2022.124209.

[33] Y. Lee, N. Tsagarakis, C. Ott, and J. Lee, "A generalized index for fault-tolerant control in operational space under free-swinging actuation failure," *IEEE Robot. Autom. Lett.*, vol. 7, no. 2, pp. 1486–1493, Apr. 2022, doi: 10.1109/LRA.2022.3140425.

[34] M. Van, "An enhanced robust fault tolerant control based on an adaptive fuzzy PID-nonsingular fast terminal sliding mode control for uncertain nonlinear systems," *IEEE/ASME Trans. Mechatronics*, vol. 23, no. 3, pp. 1362–1371, Jun. 2018, doi: 10.1109/TMECH.2018.2812244.

[35] R. K. Subroto, C. Z. Wang, and K. L. Lian, "Four-wheel independent drive electric vehicle stability control using novel adaptive sliding mode control," *IEEE Trans. Ind. Appl.*, vol. 56, no. 5, pp. 5995–6006, Sep. 2020, doi: 10.1109/TIA.2020.2977598.

[36] J. Zhang, Y. Yang, M. Hu, Z. Yang, and C. Fu, "Longitudinal–vertical comprehensive control for four-wheel drive pure electric vehicle considering energy recovery and ride comfort," *Energy*, vol. 236, Dec. 2021, Art. no. 121417, doi: 10.1016/j.energy.2021.121417.

[37] Y. Yan, J. Yang, C. Liu, M. Coombes, S. Li, and W.-H. Chen, "On the actuator dynamics of dynamic control allocation for a small fixed-wing UAV with direct lift control," *IEEE Trans. Control Syst. Technol.*, vol. 28, no. 3, pp. 984–991, May 2020, doi: 10.1109/TCST.2019.2945909.

[38] S. Vera, M. Basset, and F. Khelladi, "Fault tolerant longitudinal control of an over-actuated off-road vehicle," *IFAC-PapersOnLine*, vol. 55, no. 1, pp. 813–818, May 2022, doi: 10.1016/j.ifacol.2022.04.133.

[39] G. Park, K. Han, K. Nam, H. Kim, and S. B. Choi, "Torque vectoring algorithm of electronic-four-wheel drive vehicles for enhancement of cornering performance," *IEEE Trans. Veh. Technol.*, vol. 69, no. 4, pp. 3668–3679, Apr. 2020, doi: 10.1109/TVT.2020.2978099.

[40] B. Zhao, N. Xu, H. Chen, K. Guo, and Y. Huang, "Design and experimental evaluations on energy-efficient control for 4WIMD-EVs considering tire slip energy," *IEEE Trans. Veh. Technol.*, vol. 69, no. 12, pp. 14631–14644, Dec. 2020, doi: 10.1109/TVT.2020.3032377.

[41] L. Jin, Z. Zhang, J. Li, and J. Wang, "Fail-operation control of in-wheel motor drive electric vehicle based on wheel isolation and yaw moment compensation," *Energies*, vol. 13, no. 12, p. 3214, Jun. 2020.

[42] L. Zhai, C. Wang, Y. Hou, and C. Liu, "MPC-based integrated control of trajectory tracking and handling stability for intelligent driving vehicle driven by four hub motor," *IEEE Trans. Veh. Technol.*, vol. 71, no. 3, pp. 2668–2680, Mar. 2022, doi: 10.1109/TVT.2022.3140240.

[43] W. Zhang, Z. Wang, L. Drugge, and M. Nybacka, "Evaluating model predictive path following and yaw stability controllers for over-actuated autonomous electric vehicles," *IEEE Trans. Veh. Technol.*, vol. 69, no. 11, pp. 12807–12821, Nov. 2020, doi: 10.1109/TVT.2020.3030863.

[44] Z. Zhang, L. Zheng, Y. Li, S. Li, and Y. Liang, "Cooperative strategy of trajectory tracking and stability control for 4WID autonomous vehicles under extreme conditions," *IEEE Trans. Veh. Technol.*, vol. 72, no. 3, pp. 3105–3118, Mar. 2023.

[45] R. Wang and J. Wang, "Fault-tolerant control with active fault diagnosis for four-wheel independently driven electric ground vehicles," *IEEE Trans. Veh. Technol.*, vol. 60, no. 9, pp. 4276–4287, Nov. 2011.

[46] X. Xia, E. Hashemi, L. Xiong, and A. Khajepour, "Autonomous vehicle kinematics and dynamics synthesis for sideslip angle estimation based on consensus Kalman filter," *IEEE Trans. Control Syst. Technol.*, vol. 31, no. 1, pp. 179–192, Jan. 2023, doi: 10.1109/TCST.2022.3174511.

[47] X. Lyu, B. Hu, K. Li, and L. Chang, "An adaptive and robust UKF approach based on Gaussian process regression-aided variational Bayesian," *IEEE Sensors J.*, vol. 21, no. 7, pp. 9500–9514, Apr. 2021, doi: 10.1109/JSEN.2021.3055846.

XUN HUANG received the B.S. degree in vehicle engineering from the Fujian University of Technology, Fuzhou, Fujian, China, in 2021, where he is currently pursuing the M.S. degree in mechanical engineering.

His research interests include state estimation and dynamics control of electric vehicles.

YUNFEI ZHA received the B.S. degree in vehicle engineering from Tongji University, Shanghai, China, in 2002, and the Ph.D. degree in vehicle engineering from Hunan University, Changsha, China, in 2010.

In 2019, he was a Visiting Scholar with the Department of Mechanical and Aerospace Engineering, Carleton University, Ottawa, ON, Canada. He is currently an Associate Professor with the School of Mechanical and Automotive Engineering, Fujian University of Technology, Fuzhou, China. His current research interests include vehicle dynamics and control, intelligent vehicle, and new energy vehicle.

XIAOLONG LV received the B.S. degree in vehicle engineering from the Henan University of Science and Technology, Luoyang, China, in 2020. He is currently pursuing the M.S. degree in mechanical engineering with the Fujian University of Technology, Fuzhou, Fujian, China.

His research interests include state estimation and dynamics control of electric vehicles.

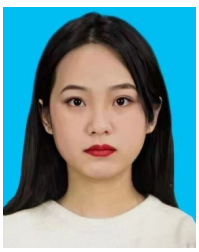

XIAOYU QUAN received the B.S. degree in vehicle engineering from Xinxiang University, Xinxiang, China, in 2019. She is currently pursuing the M.S. degree in mechanical engineering with the Fujian University of Technology, Fuzhou, Fujian, China.

Her research interest includes the torque allocation control of the 4WID EVs with the motor faults.